

## Article

# The Long-Term Deep Loessal Sediments of Northeast China: Loess or Loessal Paleosols?

Zhong-Xiu Sun <sup>1,2</sup>, Nai-Wen Zhang <sup>2</sup>, Ying-Ying Jiang <sup>3</sup>, Qiu-Bing Wang <sup>2,\*</sup> and Gan-Lin Zhang <sup>1,4,5,\*</sup>

<sup>1</sup> State Key Laboratory of Soil and Sustainable Agriculture, Institute of Soil Science, Chinese Academy of Sciences, Nanjing 210008, China; zhongxiusun@syau.edu.cn

<sup>2</sup> College of Land and Environment, Shenyang Agricultural University, Shenyang 110866, China

<sup>3</sup> Shenyang Institute of Technology, Shenyang 113122, China; yingyingjiang9111@163.com

<sup>4</sup> University of Chinese Academy of Sciences, Beijing 100049, China

<sup>5</sup> Key Laboratory of Watershed Geographic Sciences, Nanjing Institute of Geography and Limnology, Chinese Academy of Sciences, Nanjing 210008, China

\* Correspondence: qbwang@syau.edu.cn (Q.-B.W.); glzhang@issas.ac.cn (G.-L.Z.);  
Tel.: +86-157-3400-5989 (Q.-B.W.); +86-136-0140-5982 (G.-L.Z.)

**Abstract:** Previous research assumed deep buried loess as the initial composition of the overlying paleosol and failed to address the long-term continuous pedogenic weathering history in the deep loess-paleosol sequence, which was attributed to little understanding on the difference between loess and paleosol in the long-term deep loess-paleosol sequence. To distinguish between the loess and paleosol, in the long-term deep loess-paleosol sequence in northeast China, the morphology, dust deposition fluxes, geochemical characteristics, magnetic susceptibility, and grain size distributions were investigated. Results showed that the loess layers buried at depth could be differentiated from the paleosol by their poor pedogenic development. The presence of coarser grains in the loess as well as lesser amounts of clay and Fe–Mn coatings compared to paleosol indicated weaker weathering of the loess. Also, optical iron clay films deposited on the surface of the skeleton particles were less visible in the loesses than in the paleosols. From the loess evolution perspective, the pedogenic formation process of the newly formed loess soils should be considered as important as that of the reddish paleosol layer based on criteria of formation time, depth within profile, and morphological characteristics. The formation of the reddish or yellowish paleosol layer was constrained by pedogenic environments associated with climatic change and by the relative rates of deposition and pedogenesis. The terms “loessal paleosol” and “loessal paleosol sequence” are suggested to aid in systematically and consistently addressing the long-term pedogenic weathering evolution recorded in the complex formation of deep loess and paleosol sequences in pedology research. The long-term deep loessal sediments of Northeast China are loessal paleosols, which cannot be simply used as a reference for the overlying paleosol and be deducted from pedogenesis consideration.

**Keywords:** paleosol; pedogenesis; loessal paleosol; loessal paleosol sequence



**Citation:** Sun, Z.-X.; Zhang, N.-W.; Jiang, Y.-Y.; Wang, Q.-B.; Zhang, G.-L. The Long-Term Deep Loessal Sediments of Northeast China: Loess or Loessal Paleosols? *Quaternary* **2023**, *6*, 53. <https://doi.org/10.3390/quat6040053>

Academic Editors: Slobodan B. Marković and Jef Vandenberghe

Received: 14 February 2023

Revised: 14 September 2023

Accepted: 22 September 2023

Published: 7 October 2023



**Copyright:** © 2023 by the authors. Licensee MDPI, Basel, Switzerland. This article is an open access article distributed under the terms and conditions of the Creative Commons Attribution (CC BY) license (<https://creativecommons.org/licenses/by/4.0/>).

## 1. Introduction

The loess covers around 6% the global land area [1]. It is characterized as a loose aeolian deposit of yellowish silt-sized dust that mostly formed during the Quaternary Period and has a homogenous and porous structure consisting primarily of quartz and feldspar grains [1–5]. The term “soil-like aeolian” loess is often used to refer to yellowish loess deposits to distinguish them from the strict soil concept definition [4,6]. However, during certain periods the loess deposition may have been interrupted or the pedogenesis may have exceeded the loess deposition rates. Thus, the surficial loess may have experienced biological activity and physicochemical weathering and gradually developed into soil. As a result, many buried soil layers commonly appeared in the loessal sediment sequence following loess deposits. The buried soils in the loessal sediment sequence have been

termed “paleosols” [2]. This distinction was necessary to explain their formation under past natural landscape conditions [7,8] and so differentiate them from current modern natural pedogenesis. The loess deposits were transported by the East Asian monsoon, usually from arid and semi-arid source regions to the loess accumulation areas [1,2,8]. The rates of loess deposition and paleosol pedogenesis corresponded to the strength of winter monsoons and summer monsoons, respectively [9,10]. The loess-paleosol sequence recorded quasi-continuous Quaternary climatic changes across the 2.6 Ma [2,11–14].

The striking difference between the yellowish loess and the reddish paleosol has been attributed to greater proportions of stable minerals in paleosols relative to unstable minerals due to pedogenic weathering in paleosols [3,15] and especially to the concentration, mineralogy and smaller grain size of the magnetic carriers in paleosols [16,17]. The pedogenesis was mainly controlled by the precipitation and temperature related to the intensity of Asian summer monsoons [3,11]. The loess experienced weaker pedogenesis compared to the paleosol [6,15] and usually had greater carbonate content [18]. Upper loess mantles affected by surficial processes had been figured out differences between loess and paleosol, albeit long-term deep loesses and paleosols pedogenesis are limited [15]. To quantify the pedogenic changes, the loess was assumed to represent the initial composition of the overlying paleosol [2,3,19]. According to this assumption, the material migrations and transformations in paleosols have a different starting point compared to loess, allowing for an unbiased comparison between the two. However, characterizing the weathering evolution in the loess-paleosol sequence transition boundary as continuous cannot be addressed under this assumption.

Although the pedogenesis has been synchronized with loess deposits in the loess-paleosol sequence [20], the deposited loess grains have been modified to various degrees by pedogenesis, masking or diluting the original winter monsoon influence in the grain size composition [14]. The loess also may have been potentially influenced by material translocations from the overlying layers. Thus, pedogenesis combined with translocation processes may have complicated a clear loess-paleosol sequence separation and caused potential deviations in reconstructing past climate history. In order to capture the pedogenic effect, macro- and micro-morphological observations and chemical and mineralogical analyses including illuvial clay on thin sections and quantitative chemical weathering intensity have been centered on discontinuous samples and used to quantitatively assess paleosol pedogenesis [21–24]. However, there is little research on loess pedogenesis to support the assumption that this un-weathered parental loess can be used as a reference for the overlying paleosol and be deducted from pedogenesis consideration. The term “loess”, which is synonymous with sediment in studies on “loess-paleosol sequence” evolution [5,25], seems relatively simple and intuitive but fails to address the possibility that pedogenesis may have occurred in the loess, albeit limited.

Loess pedogenesis is as equally important as paleosol pedogenesis in the study of the loess-paleosol sequence when addressing the role of pedogenesis on paleoclimate and continental evolution. The objective of this study was to distinguish between the loess and paleosol and provide suggestions for refining the terminology used to describe the pedogenesis of loess and paleosols. We first characterized the morphology, dust deposition fluxes, geochemical characteristics, magnetic susceptibility, and grain size distributions in loess and paleosols. Then evidence for apparent illuvial clay on thin sections and quantitative chemical weathering intensity were evaluated to gain more insight into the potential difference between loess and paleosol pedogenesis. And we compared our results with data from other research and pointed out similarities to better reveal the difference between loess and paleosols according to the criteria of identification of paleosols. Lastly, we discussed the merits of using the term “loessal paleosol” instead of “loess” to recognize the presence of pedogenesis. Similarly, we discussed the use of “loessal paleosol sequence” instead of “loess-paleosol sequence”.

## 2. Materials and Methods

### 2.1. The Study Area and Profile Descriptions

Chaoyang City is located in the Liaoning Province in northeast China's loess distribution region (Figure 1). The area belongs to the North Temperate Zone and has a continental monsoon climate. The mean annual temperature at Chaoyang is 9 °C, and the mean annual precipitation is 450–500 mm.

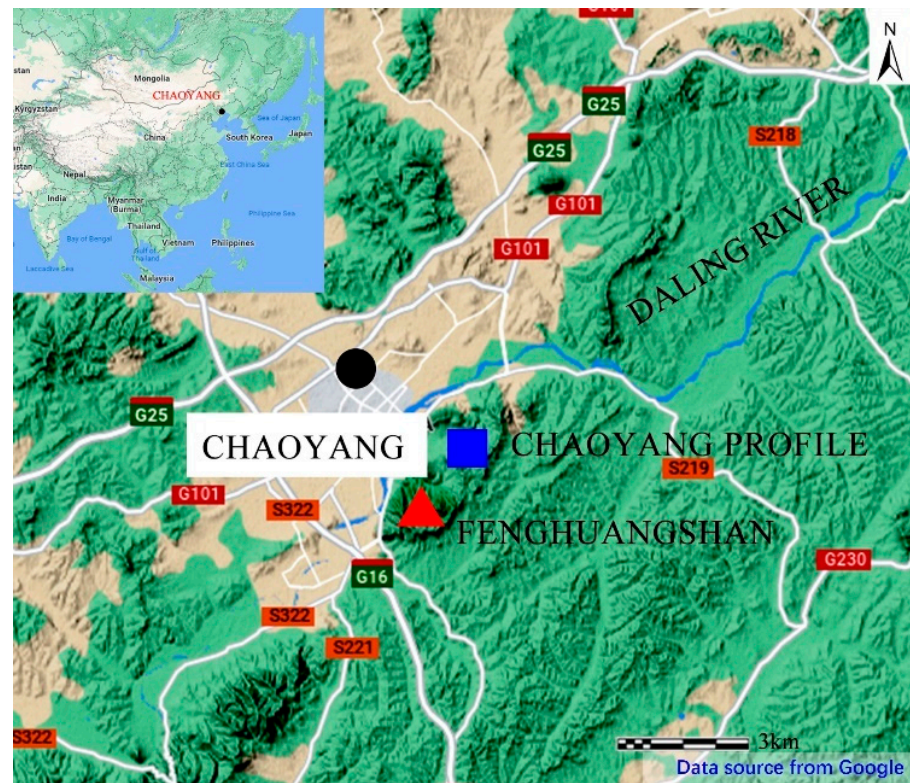


**Figure 1.** Schematic map presenting the location of the Chaoyang loess-paleosol profile. The black solid circle on the inset map shows the location of Chaoyang in China. The red triangle and blue square represent the Fenghuangshan mountain and Chaoyang profile, respectively.

Chaoyang's geotectonic structure is part of the North China platform. Two Archean tectonic strata dating to the pre-Sinian period constitute the stratigraphic basement in the area. The lower tectonic stratum is partly exposed in the Inner Mongolia tectonic zone of the Earth's axis, and consists of granite, metamorphic rock, biotite, gneiss, and hornblende gneiss. The upper tectonic stratum consists of shallow metamorphic schist, marble, and phyllite, and is mainly distributed along the Daling River. The stratigraphic basement is covered by Paleozoic sediment and represents the main stages of tectonic development in this region. The Paleozoic sedimentary cover consists mainly of limestone and dolomite, formed during the Cambrian and Ordovician periods. Roughly, the Sinian shallow metamorphic rocks are distributed in the mountain top, and Cambrian and Ordovician limestone and mica are mainly distributed in the middle and lower parts of the mountain [26–28]. The Chaoyang profile originated from windblown dust and has no pedogenic relationship with the underlying basal layer [20].

The Chaoyang profile is 19.85 m in depth, and its bottom boundary has not been investigated. It is located in a well-defined closed basin and is less influenced by flowing water (Figure 1). The profile is located at a stable flat place at the mid-point of the Song-Ling Ridge in the hilly area, which has a small catchment area [26]. No evidence of human influence or accelerated erosion has been found. Therefore, a relatively complete-representative set of aeolian dust with varying thicknesses has been preserved here since

the late middle Pleistocene. Hiatuses and erosions were thus supposed to be few in the studied profile. The Chaoyang profile consists of the loess (L)-paleosol (S) sequence S0, L1, S1, L2, S2, L3, S3, L4, S4, and L5. S0 is a brown zonal soil layer (cinnamon soil classified as a Haplustalf according to the U.S. Soil Taxonomy [29]) located at the top of the Chaoyang profile. Underlying S0, four reddish stratigraphic layers (S1–S4) are interbedded with five yellowish stratigraphic layers (L1–L5) (Figure 2). The boundaries between adjacent layers are clear. Profile morphologies were described in detail according to the “Field book for Describing and Sampling Soils, version 3.0” [30]. A horizon of sub-rounded coarse limestone gravel less than 7 cm thick was observed at the bottom of S0, beneath the L1 horizon, indicating a substantial environmental change. There was a stepwise change in soil texture from the loam and silt loam to the sandy loam with depth of 0–195 cm. Silt particle size class uniformly distributed across the depth of 228–1985 cm which was derived from a same eolian source. A silt loam transitional shift was found between them at the depth of 195–228 cm. An abrupt color varied from 10 YR to 2.5 YR at 228 cm with a transitional 5 YR color shift. Due to the presence of complexly mixed materials, the upper part of the Chaoyang profile (UPP, 0–195 cm) and the middle part (MIP, 195–228 cm) were not considered in the study, only the lower part (LOP, 228–1985 cm) [20].

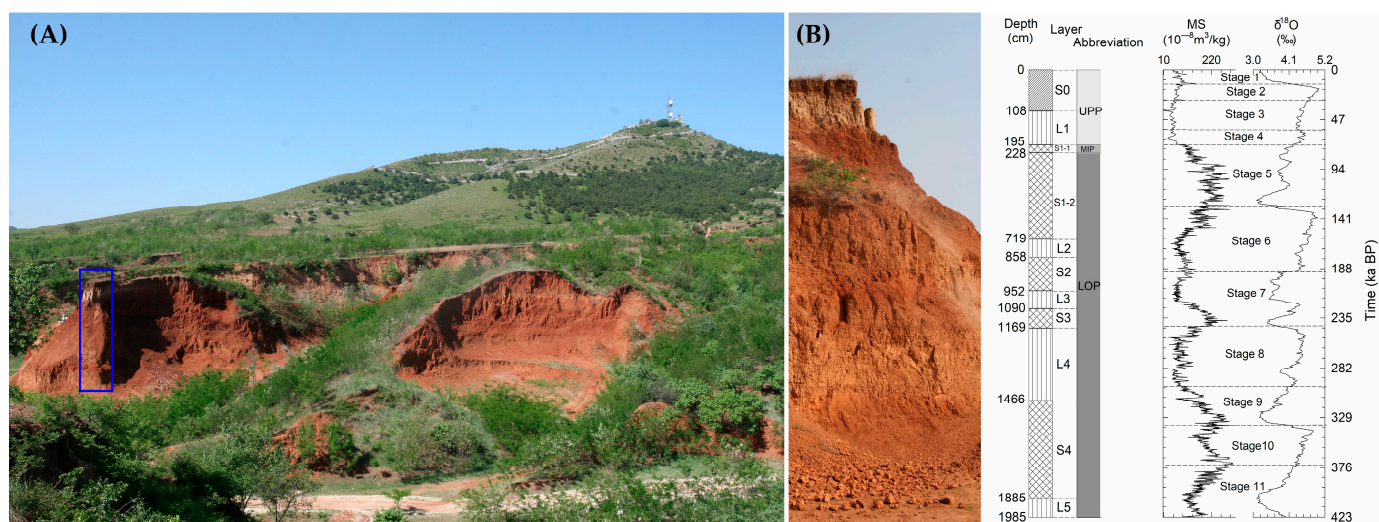


**Figure 2.** (A) The associated landscape photo of the Chaoyang profile, and (B) the Chaoyang profile photo and the schematic representation of its stratigraphy with corresponding time constraints where “L” indicates loess and “S” indicates paleosol. The blue rectangle on (A) shows the location of the Chaoyang profile. The data on age for the plot are cited from Chen, Wang, Han and Wu [31]. The chronostratigraphic data were obtained by using 10 reliable age controls interpolated by using the model of susceptibility and accumulation rate, and then its interpretations were addressed by relating with the Marine Oxygen Isotope Stratigraphy of SPECMAP (data cited from a reference [32] Lisiecki and Raymo, 2007). The marine oxygen isotope record of SPECMAP  $\delta^{18}\text{O}$  was subdivided into 11 stages (MIS) since 423 ka BP [32]. Note: S0 represents modern soil. The upper part (0–195 cm), middle part (195–228 cm), and lower part of the observed profile (228–1985 cm) were abbreviated as UPP, MIP, and LOP, respectively.

## 2.2. Sampling Methods

Forty-two bulk samples from pedogenic horizons were collected for chemical and physical analysis, and 946 sub-samples were taken at 2-cm intervals from the surface to the bottom of each horizon in the field to determine grain size distributions as well as magnetic susceptibility. Ten samples for dating were collected along the layer boundaries. Intact oriented core samples about 15 cm long were collected from selected horizons for thin sections. Natural clods were sampled from each pedogenic horizon for bulk

density determinations. All samples were preserved in desiccators under a dry, ventilated, pollution-free environment with no direct sunlight before analysis.

### 2.3. Laboratory Methods

Soil powder samples were air-dried and then ground to pass through nylon sieves to prepare samples in different sizes according to the requirements of different subsequent analyses. The outer 2-cm part of oriented core samples was removed and remaining central parts were impregnated with epoxy resin to prepare thin sections. First, decimeters from two ends of dating samples in aluminum tubes were removed to avoid light contamination under a dark-room condition. The 200-mesh soil powder samples and X-ray fluorescence for major elemental composition [33], the oriented core samples and standard thin section techniques [34] and terminology [35] for micro-morphologies, the clod method for soil bulk density [36], the 100-mesh (150  $\mu\text{m}$ ) soil powder samples and wet oxidation method for soil organic carbon (SOC) [37], the 10-mesh (2000  $\mu\text{m}$ ) soil powder samples and grain size analytical procedure for grain size composition [38], optically stimulated luminescence, and the 10-mesh (2000  $\mu\text{m}$ ) soil powder samples and a Bartington susceptibility meter (MS2) equipped with a MS2F probe for magnetic susceptibility were employed (Bartington Instruments, Witney, UK). The ten dating samples with control significance were dated by Chen et al. [39] without time reversal problems. Then 10 reliable age controls were interpolated by using the model of susceptibility and accumulation rate with age [11,40] to build the chronostratigraphic data shown in Figure 2. And then its interpretations were addressed by relating with the Marine Oxygen Isotope Stratigraphy of SPECMAP (data cited from Lisiecki and Raymo, 2007) in Figure 2. The marine oxygen isotope record of SPECMAP  $\delta^{18}\text{O}$  was subdivided into 11 stages (MIS) since 423 ka BP [32]. They were stratigraphically correlated well with that in the Xifeng profile [41]. For example, the 243–311 ka BP paleosol layer in the Xifeng profile correlated with the L4 in the Chaoyang profile which has been formed 243–311 ka BP. The recorded climate trends indicated by Loesses (L) interbedded with paleosols (S) can be globally well correlated [2], while the numbers following “L” and “S” had regional features when correlating with others may need careful comparisons due to loess strata, terminations that varied in different regions, and researchers’ different subjective judgment.

Evidence for apparent illuvial clay on thin sections and vertical distributions of geochemical features were evaluated to provide more insight into the potential difference between the loess and paleosols. Standard soil samples of GBW(E)-070042 and GBW(E)-070041 commonly used in China were added and determined during chemical measurements for monitoring the analysis quality with the standard deviation less than 3% and relative errors less than 5% for a random sample in triplicate. Detailed descriptions of all the laboratory methods can be found in publications of previous studies [20,42].

The Munsell Soil-Color Charts were used to determine representative soil color for each horizon. The Munsell color was then converted to the redness rating (RR) using the formula  $RR = (10-H) \times C/V$  [43], where H is hue and C and V are Munsell chroma and value, respectively. For example, the hues 10 YR, 7.5 YR, 5 YR, 2.5 YR, and 10 R, translate to H values of 10, 7.5, 5, 2.5, and 0, respectively. The hue symbol is the letter abbreviation of the rainbow color including YR for Yellow-Red, R for Red, and Y for Yellow preceded by numbers from 0 to 10. Higher hue values mean lower RR values. The Chemical Index of Alteration (CIA) and the Na/K ratio were used to quantify the chemical weathering of soils. The computational formulas for these indices have been summarized with detailed definitions in a previous paper [44]. The mineral dust flux ( $\text{g m}^{-2} \text{yr}^{-1}$ ) was calculated using the formula summarized by Feng, Hu and Chen [45].

Necessary descriptive statistics for data of chemical measurements were performed in SAS procedure (SAS Institute, 2000).

### 3. Results

#### 3.1. Profile Morphologies

##### 3.1.1. Field Morphology

L4 was the thickest L layer with obvious “red-colored soil coated yellow soil” characteristics present in the upper part, while the lower part was light yellow and orange and had vertical joints and large pores. Few clay lined pores and common clay and Fe–Mn coatings were also observed in the top and bottom parts. L2 and L3 were thinner and had more clay and Fe–Mn coatings compared to L4, indicating stronger pedogenesis. The partially investigated L5 at the bottom of the profile had no obvious pedogenic morphological characteristics across the entire thickness and appeared to be uniform. The morphological characteristics of the L layers, especially L2 and L3, were similar to those of S1 and S4 (paleosols). The L layers also had well developed structure with rich Fe–Mn and clay coatings along structural ped faces and the inner walls of pores. However, greater amounts of clay and Fe–Mn coatings in Bt horizons were observed in the paleosols. S1 and S4 were thicker compared to S2 and S3 and altogether showed no signs of erosive or unconformity surfaces.

Uniform silt distribution across the LOP (228–1985 cm) underlined the transitional shift to silt loam in S1-1 (195–228 cm) in the MIP. An abrupt color alternation from 10 YR (UPP) to 2.5 YR (LOP) appeared with a 5 YR transitional shift at a depth of 228 cm (MIP). Colors alternated between bright red brown and orange in the LOP. The loess generally had lower redness ratings, indicating weaker rubification compared to the overlying paleosol (Figure 3).

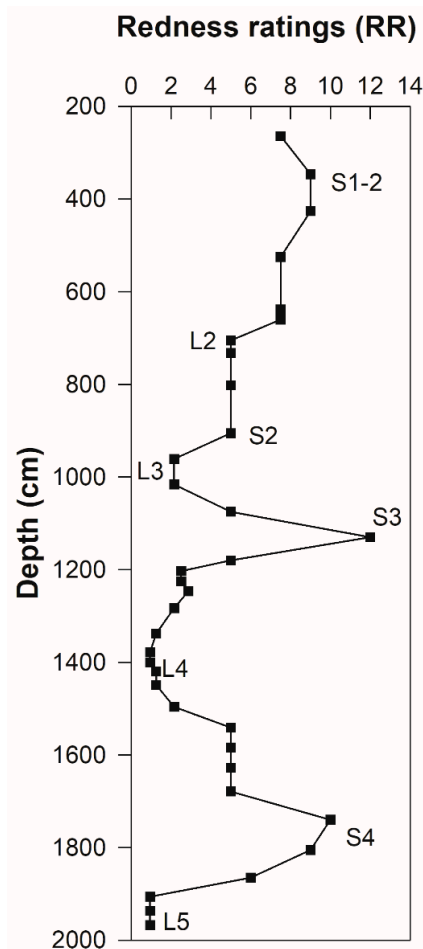


**Figure 3.** The redness ratings (RR) with depth for the lower part of the Chaoyang profile (LOP, 228–1985 cm). The “L” indicates loess and “S” indicates paleosol.

### 3.1.2. Micromorphology

The matrix was uniform across the LOP, and no evidence of vertical stratification could be detected (Figure 4). Fabrics in the loess and paleosol horizons were similar.

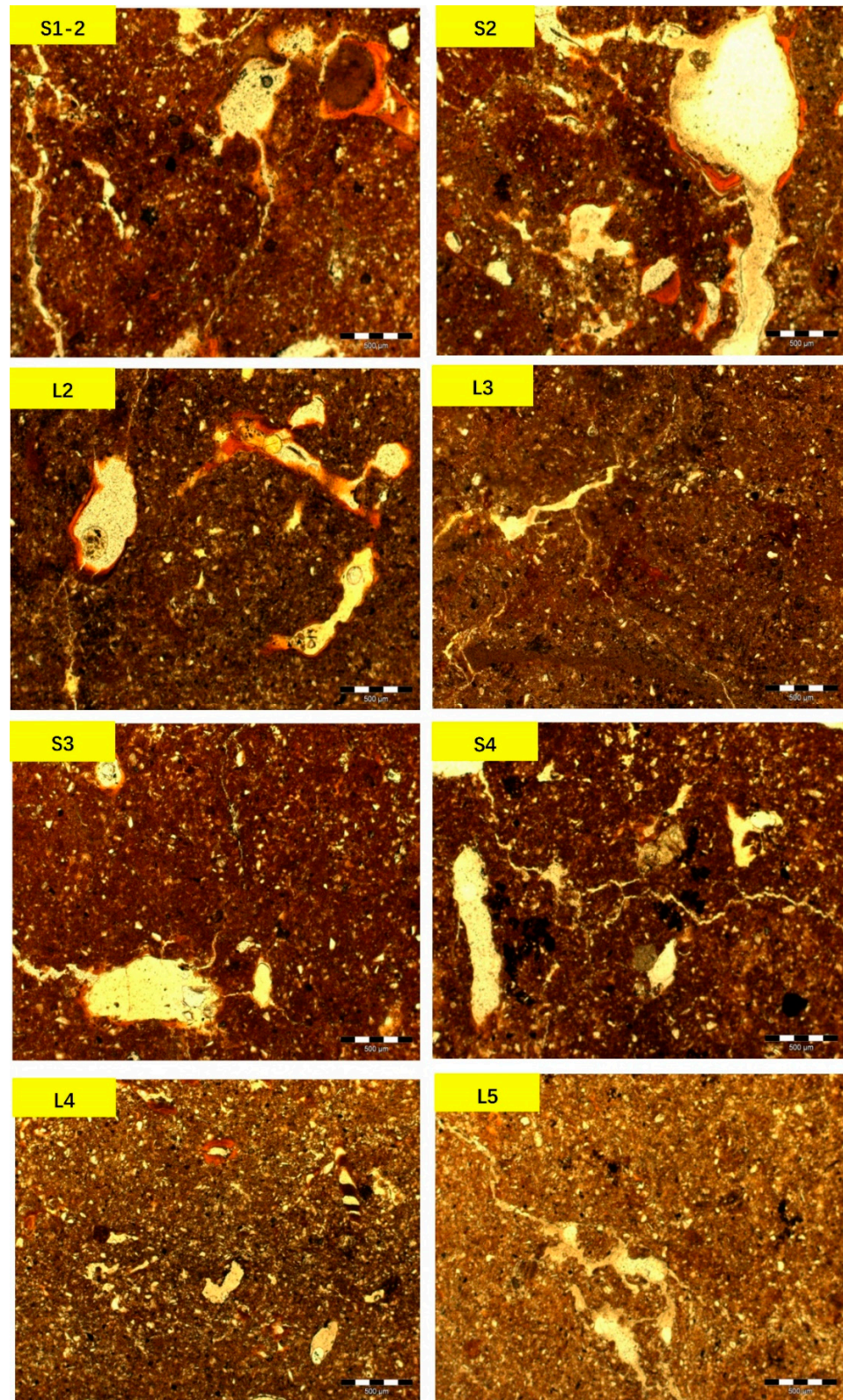


**Figure 4.** Thin section micrographs of different horizons in the lower part of the Chaoyang profile (LOP, 228–1985 cm), under a single polarized light. The “L” indicates loess and “S” indicates paleosol.

Different amounts of illuvial clay and Fe–Mn coatings along pores were detected in the loess, and overall, there were fewer than in the paleosols. Depleted clay and Fe–Mn oxides in coarse textured zones in pale yellow color appeared in both the loess and paleosols. Coarser silt fragments were observed, especially in the channels of paleosols, compared to the matrix. Also, more striated clay on channel walls and ped faces was detected in the paleosols compared to the loess. The matrix showed a stronger rubification in the paleosols compared to the underlying loess. The bottom loess layer (L5) had simple packing voids and no indicators of pedogenic development. Except for L5, the loess layers (L2–L4) have experienced weak pedogenesis.

### 3.2. Dust Deposition Fluxes

The mineral dust flux of aeolian deposits in the LOP was approximately  $69.68 \text{ g m}^{-2} \text{ yr}^{-1}$ . However, as expected, the loess had a greater average mineral dust flux, at  $77.74 \text{ g m}^{-2} \text{ yr}^{-1}$ , compared to the paleosol, at  $65.29 \text{ g m}^{-2} \text{ yr}^{-1}$ . Paleosols were characterized consistently by lower values for mineral dust flux compared to the loess overlying or underlying them (Figure 5).

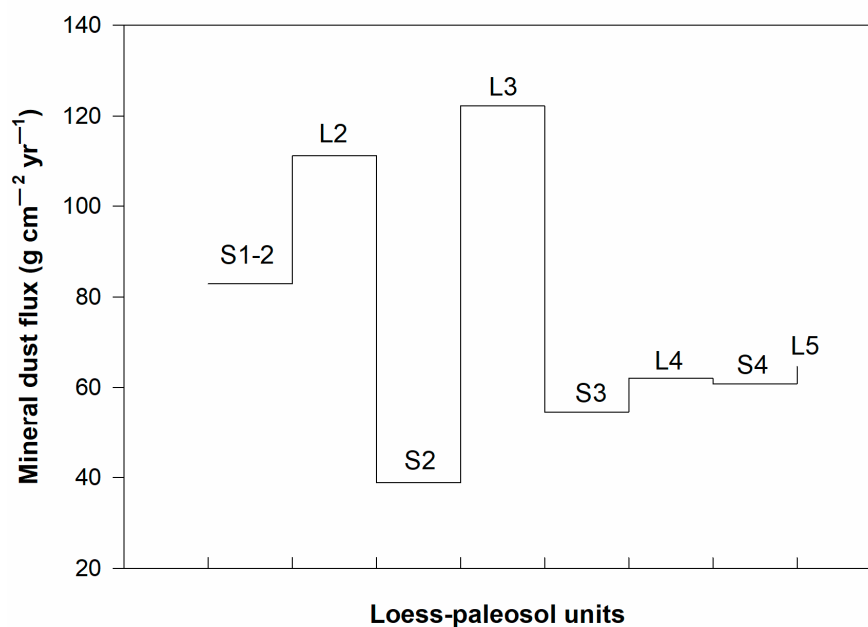


**Figure 5.** Mineral dust flux of loess and paleosols in the lower part of the Chaoyang profile (LOP, 228–1985 cm). The “L” indicates loess and “S” indicates paleosol.

### 3.3. Geochemical Characteristics

Except for  $\text{Na}_2\text{O}$ ,  $\text{P}_2\text{O}_5$ , and  $\text{CaO}$ , the distribution curves of major elements in the loess and paleosols were nearly flat and close to the AUCC (the average upper continental crust) curve, indicating a similar chemical composition between the LOP and AUCC (Figure 6). This reflects a genetic link between loess in terms of aeolian dust deposits and the upper continental crust, indicating a transported and well mixed aeolian dust that gradually approached the average composition of the upper continental crust. However, the data shows that the amount of  $\text{Na}_2\text{O}$ ,  $\text{P}_2\text{O}_5$ , and  $\text{CaO}$  in the loess and paleosols slightly deviated from the average value of the upper continental crust. The  $\text{CaO}$  loss in the paleosols was comparable to that in the loess, but smaller  $\text{Na}_2\text{O}$  and  $\text{P}_2\text{O}_5$  losses were found in the loess compared to the paleosols. This indicates that the loess has experienced weaker effects from pedogenesis compared to the paleosols. The total content of  $\text{SiO}_2$ ,  $\text{Al}_2\text{O}_3$ , and  $\text{CaO}$  accounted for close to 90% of total elemental composition, dominating both the loess and paleosols.

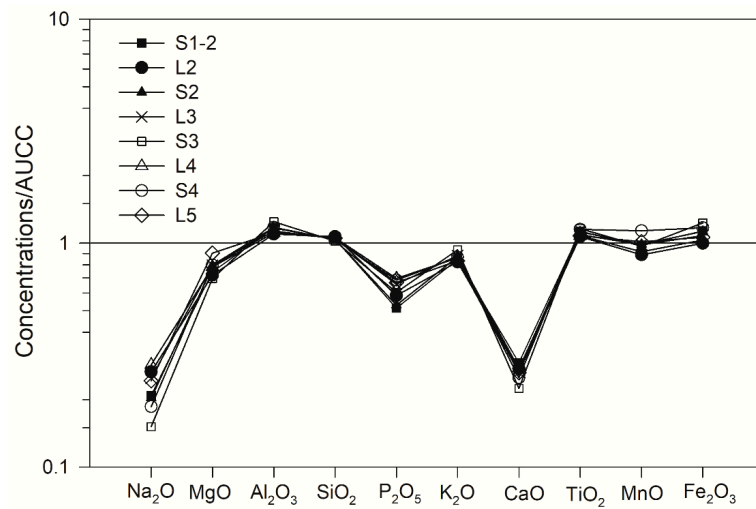


**Figure 6.** AUC-normalized pattern of major elemental distributions of loess and paleosols in the lower part of the Chaoyang profile (LOP, 228–1985 cm). The AUCC (the average upper continental crust) was cited from Rudnick and Gao [46]. The “L” indicates loess and “S” indicates paleosol.

The CIA of the LOP ranged from 73 to 82 (Figure 7). The average CIA value for the paleosols was 80 (std. dev. = 1.2), which was greater than that of the loess, an average of 76 (std. dev. = 1.3). The average CIA value for the LOP, at 78, was greater than that of the AUCC, which was 52.74 [46]. The average Na<sub>2</sub>O/K<sub>2</sub>O ratio for the loess was 0.57 (std. dev. = 0.07) and only 0.38 (std. dev. = 0.06) for the paleosols. The CIA curves and Na<sub>2</sub>O/K<sub>2</sub>O ratios showed a weathering trend that was stronger for the paleosols compared to the loess, which experienced weaker weathering effects.

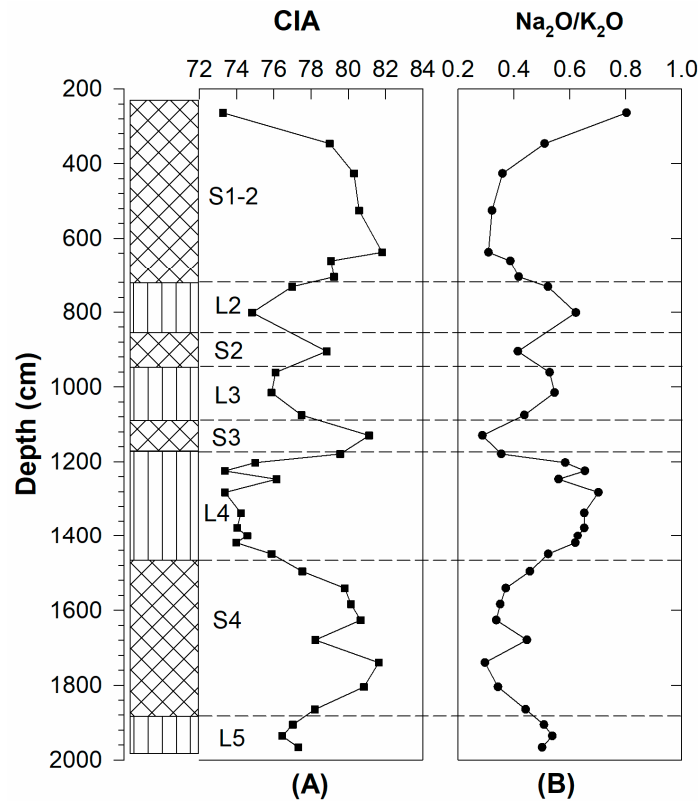


**Figure 7.** Changes of the chemical index of alteration (CIA) (A) and Na<sub>2</sub>O/K<sub>2</sub>O (B) with depth in the lower part of the Chaoyang profile (LOP, 228–1985 cm). The “L” indicates loess and “S” indicates paleosol.

### 3.4. The Grain Size Distribution and Magnetic Susceptibility

An extremely lower sand content (>63  $\mu\text{m}$  coarse sand) was detected in the LOP (Figure 8B). Silt sized grains dominated the LOP grain composition, with typical content of aeolian grains in the 10–50  $\mu\text{m}$  fraction varying from 43% to 86%. Clay content varied from 1% to 8%. The mean grain size of the LOP was 10–30  $\mu\text{m}$ .

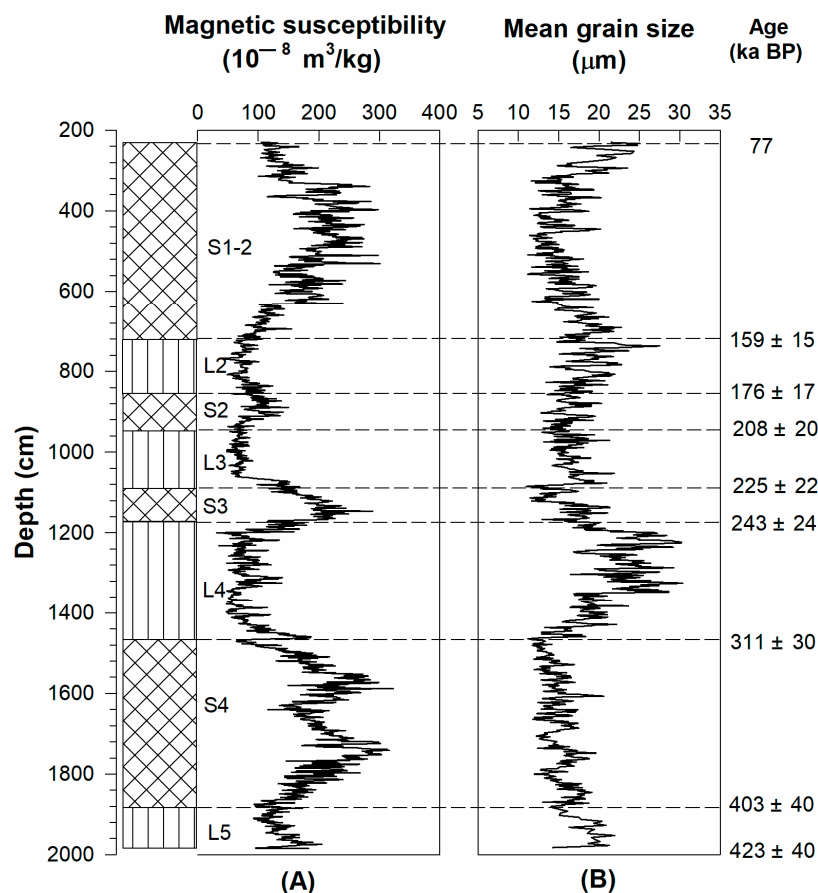


**Figure 8.** Changes of magnetic susceptibility (A) and mean grain size (B) in the lower part of the Chaoyang profile (LOP, 228–1985 cm). The “L” indicates loess and “S” indicates paleosol.

The paleosols were characterized consistently by finer mean grain sizes and greater magnetic susceptibility values compared to the loess overlying and underlying them (Figure 8). The paleosols layers had a finer mean grain size (16  $\mu\text{m}$ ) ranging from 11  $\mu\text{m}$  to 25  $\mu\text{m}$  compared to the loess (19  $\mu\text{m}$ ) that ranged from 11  $\mu\text{m}$  to 30  $\mu\text{m}$ . The magnetic susceptibility of the paleosols was higher, at  $179 \times 10^{-8} \text{ m}^3/\text{kg}$ , and varied from  $50 \times 10^{-8} \text{ m}^3/\text{kg}$  to  $323 \times 10^{-8} \text{ m}^3/\text{kg}$  while that of the loess was less, with an average value of  $92 \times 10^{-8} \text{ m}^3/\text{kg}$  and varying from  $31 \times 10^{-8} \text{ m}^3/\text{kg}$  to  $205 \times 10^{-8} \text{ m}^3/\text{kg}$ .

## 4. Discussion

### 4.1. The Identification of Paleosols

Paleosols are widely distributed across the Earth’s land surface and are defined in different ways [1]. Ruhe [7] defined the paleosol as the soil that formed under a past natural landscape, limiting the definition to mainly the time dimension. Others have defined paleosols according to the profile location, that is, deep and buried or as a geologically diagenetic petrified soil [47]. From the scientific perspective, three major terms or criteria have been used to characterize paleosols: (i) formation time, (ii) depth with profile, and (iii) morphological characteristics. A short discussion of each term and criteria follows in order to provide a scientific context and an understanding basis for other parts and

the newly proposed use of “loessal paleosol” rather than “loess” and “loessal paleosol sequence” rather than “loess-paleosol sequence”.

#### 4.1.1. The Time Criteria for Paleosol Formation

The paleosol formation time varies considerably from several hundreds to thousands of years to as much as millions to tens of millions or billions of years [48], making practical application of age as a criterion very difficult. According to Bronger and Catt [49], Ruhe’s definition for the paleosol, though more concise and widely used, was too broad and unclear regarding the specific time definition of a past natural landscape and, as a result, could inaccurately identify all soils as paleosols. In order to solve this problem, some scholars suggested setting a minimum age limit for paleosols, which was then defined as the time when changes to soil properties due to changes in one or more soil-forming factors can be detected. For example, Duchaufour [50] defined the soil that formed before the last cold period of the Pleistocene as a paleosol. This was because the soil formed during the interglacial period and commonly contained different remnant features from Holocene soils. Li et al. [47] believed that there was no absolute upper time limit for paleosols, which could be several thousand years to several billion years. It was also thought that a paleosol was a soil that has been developing for over 2000 years, while a soil that has been developing for less than 2000 years was a modern soil [51]. Lu and He [52] believed that the definition of paleosol had little relationship with the time of formation and argued that paleosols should not have a specific absolute age limit. The key for identifying a paleosol was to evaluate the changes of soil conditions instead. If soil conditions changed qualitatively and the resulting changes in soil properties could be clearly detected, the soil could be then determined as a paleosol [48].

#### 4.1.2. The Depth Criteria for Identification of Paleosols

Most countries set the depth for soil surveys at 1 m, 1.5 m, or 2 m, making it difficult to obtain information on deeper soil material. While the 2 m depth is practical for most mapping purposes, soil formation processes do not stop at 2 m [1,53]. Only in limited studies [54] related to soil-landscape relations and environmental quality has the entire weathering profile, including residual soils, been studied. Therefore, the depth of the paleosol should not be artificially limited and soil classification methods should also address deeply weathered profiles.

#### 4.1.3. The Morphological Characteristics for the Identification of Paleosols

In addition to the inclusion of a small number of loess and paleosols in geological paleosol classification, there is a general focus on consolidated diagenetic paleosols as soil fossils. While this may be useful for paleogeography, geo-history and other subjects, the use of soil fossils in soil science research applications may be limited. The solidified diagenetic paleosols that have traces of pedogenesis are more akin to rocks than soils and do not necessarily host life as soils do. Thus, we argue that petrified paleosols should not be included in the soil classification system. Although a unified soil classification system that includes paleosols is advocated, the distinction between soils and geological bodies is essential and the study of paleosols by soil scientists must be separated from the study of geo-history [51].

#### 4.2. The Difference between Loess and Paleosols

During the chemical weathering of the upper crust, the geochemical process of weathering was greatly restricted by the weathering degree of feldspar, in which alkali metal elements depleted in the form of ions and then clay minerals formed. The CIA index effectively indicated the degree of feldspar weathering into clay minerals, excluding effects from elemental migration and accumulation, and well reflected the chemical weathering condition of sediment formation [55]. The feldspar earth surface minerals, especially plagioclase, were rich in sodium while K-feldspar, illite, and mica were rich in potassium.

Sodium and potassium were alkali metal elements and had a ratio of 1:1 in the Earth's crust. However, due to a greater radius of potassium ion, the adsorption of clay to the potassium ion was greater compared to the sodium ion, resulting in greater amounts of potassium compared to sodium [56]. Therefore, the molecular molar ratio of  $\text{Na}_2\text{O}/\text{K}_2\text{O}$  could reflect the "clayization" degree [57]. The CIA and Na/K molar ratios were developed to address the weathering intensity between the loess and paleosol.

The average AUCC reflects chemically un-weathered conditions (Figure 9). The weathering degree of loess and paleosols in Lingtai (LT) and Luochuan (LC) from the China Loess Plateau was at an intermediate stage of chemical weathering. Although the Chaoyang section (CY) centered at an intermediate chemical weathering stage, CY loess and paleosols experienced stronger chemical weathering under warmer and wetter climates compared to the loess and paleosols from LT and LC. Some paleosols from CY, however, experienced extreme weathering close to that of Xuancheng red clay (XC) under hot and humid climates. The data collected showed consistently that, like paleosols, loess experienced some degree of chemical weathering, though it was less intense than that of paleosols. In loess, several indicators, such as fine grain size, amounts of clay and Fe–Mn coatings, and some clay-filled pores and fissures (Figure 4), indicate that some degree of weathering occurred. Grain size was finer in the paleosols than in the loess. The grain size distributions of the loess and paleosols showed a bimodal pattern. The principal mode and secondary mode were associated with coarse fraction (10–50  $\mu\text{m}$ ) and finer fraction (2–6  $\mu\text{m}$ ), respectively. The secondary mode range as well as grains less than 2  $\mu\text{m}$  in the paleosol were more prominent compared to losses, indicating a greater percentage of fine particles in the paleosols (Figure 10). Also, greater amounts of clay and Fe–Mn coatings were observed in paleosols compared to loess. Optical iron clay films deposited on the surface of the skeleton particles or filling pores and fissures were more visible in the paleosols (Figure 4). In other research, the Molluscan fauna was reported to appear in more diversified communities during paleosol formation than loess [58]. The carbonate content was obviously greater in the loess than that in the paleosol [18]. All this evidence indicated that loess was poorly developed relative to the paleosol.

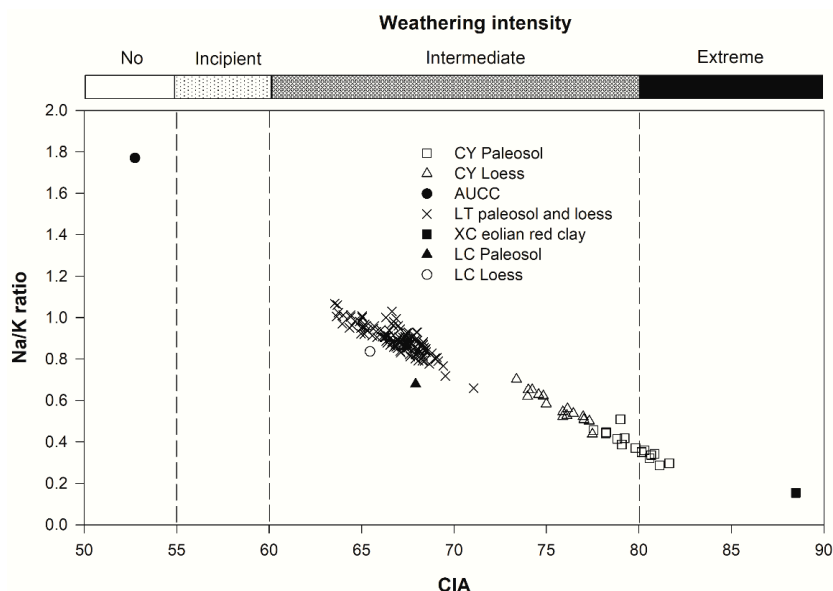


**Figure 9.** Scatter diagram of the chemical index of alteration (CIA) and Na/K molar ratio of the lower part (LOP, 228–1985 cm) in the Chaoyang profile (CY). The data of Xuancheng aeolian red clay (XC) was cited from Li et al. [56]. The elemental composition data of typical loess-paleosol sequences: the Lingtai section (LY) and the Luochuan section (LC) from the China Loess Plateau was cited from Yang, Ding and Ding [19] and Li et al. [56] and used in calculating CIA and Na/K molar ratio values. Note, the available Lingtai data cannot be separated successfully for loess or paleosols.

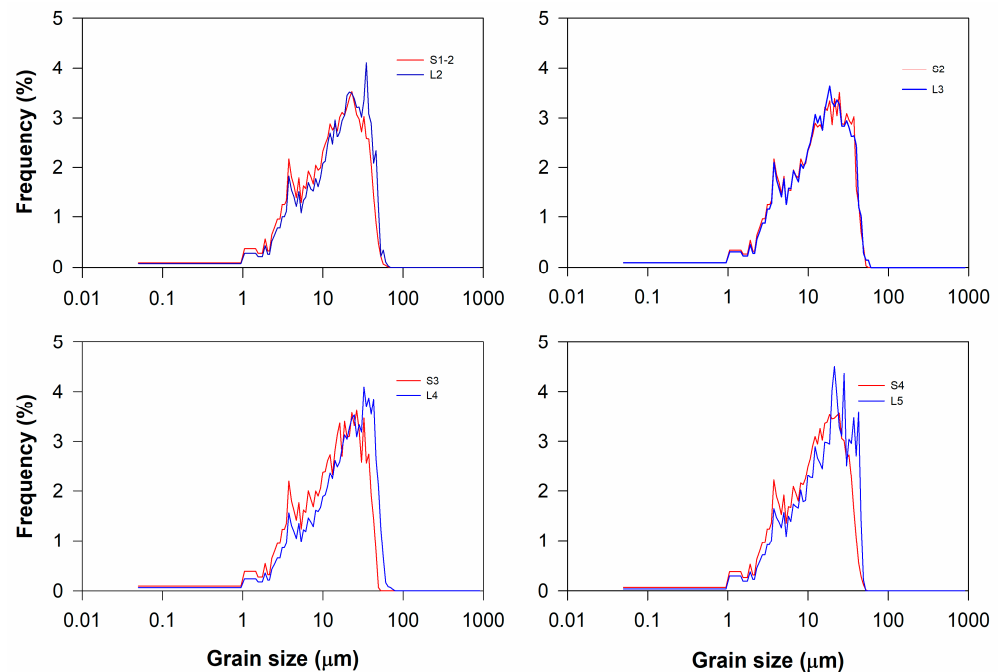


**Figure 10.** Grain size distributions of loess and paleosols in the lower part of the Chaoyang profile (LOP, 228–1985 cm). The “L” indicates loess and “S” indicates paleosol.

#### 4.3. The Suggested Definition of Loess in the Loess-Paleosol Sequence

Widely distributed loess [1], experienced the loessification process [6], commonly formed by accumulation of windblown silt dust and other formational activities [4] under different landscapes [8]. The warm, wet southeast wind accompanying East Asian summer monsoons brought abundant precipitation and heat, which promoted precipitation-driven pedogenesis in loess deposits, leading to apparent signals in magnetic susceptibility. Coarser grain size fractions were transported by strong winter winds accompanying East Asian winter monsoons, resulting in the coarser mean grain sizes detected in loess. The use of magnetic susceptibility [2,9] and grain size parameters [2,14,59–61] in reconstructing paleoclimatic monsoon evolution indicated that four alternating changes of dry-wet and cool-warm cycles occurred during the long period of geological history since the 423 ka BP Quaternary Period (Figure 8). Four yellowish loess layers were found interbedded with four reddish paleosol layers. The weakly weathered loess, which had less obvious pedogenic characteristics, was mainly regarded as parent material overlying paleosols [2]. Because there is some pedogenesis detected in loess, albeit weaker compared to paleosols, from the loess evolution perspective, the pedogenic formation process of the newly formed loess soils should be evaluated in the same manner as the reddish paleosol layer, i.e., based on criteria of time of formation, depth within profile, and morphological characteristics. Such recognition could be important for correctly identifying climate change sequences, since the formation of a reddish or yellowish paleosol layer is clearly constrained by pedogenic environments associated with climatic change and by the relative rates of deposition (Figure 5) and pedogenesis (Figure 9) associated with alternating warm-wet and cold-dry cycles. The reddish paleosol layers formed under warm and wet climates when there were lower rates of deposition and active pedogenesis with strong chemical weathering, while the yellowish paleosol layers formed under cold, dry climates when there were greater rates of deposition and weak weathering. The term “loess”, which is synonymous with sediment in studies on “loess-paleosol sequence” evolution [5,25], seems relatively simple and intuitive but fails to address the possibility that pedogenesis may have occurred in the loess, albeit limited. A more precise explanation should be suggested. Thus, we suggest that the term “loessal paleosol sequence” be used instead of “loess-paleosol sequence” to

recognize the occurrence of pedogenesis in loess deposits in pedology especially in research trying to reveal the long-term pedogenesis evolution recorded in the complex formation of loess and paleosol sequences. We strongly understand that the terminology change from “loessal paleosol” instead of “loess” is not apt turn due to much more necessary basis needed than provided in the research. However, the suggested new definition characterizes the loessal paleosol sequence as the superposition of a series of pedogenic layers with different degrees of soil pedogenesis that were derived from loess parent materials under different climatic environments in the pedology world.

## 5. Conclusions

The loess in the loess-paleosol sequence is identified as the yellowish paleosol layer at different pedogenic weathering stages. The formation of the reddish or yellowish paleosol layer is constrained by pedogenic environments associated with climatic change and by the relative rates of deposition and pedogenesis. The yellowish paleosol layer buried at depth can be differentiated from the reddish paleosol layer by the relatively poor development of loess. The loessal sediments of Northeast China are loessal paleosols, which cannot be simply used as a reference for the overlying paleosol and be deducted from pedogenesis consideration. An appropriate method of selecting an initial composition for the loessal paleosol sequence is the challenge of addressing the continuous pedogenic weathering history.

**Author Contributions:** Conceptualization, Z.-X.S., Q.-B.W. and G.-L.Z.; methodology, Y.-Y.J., Z.-X.S., Q.-B.W., G.-L.Z. and N.-W.Z.; software, Z.-X.S., Y.-Y.J. and N.-W.Z.; validation, Z.-X.S., Q.-B.W. and G.-L.Z.; formal analysis, Z.-X.S., Y.-Y.J. and N.-W.Z.; investigation, Q.-B.W. and Z.-X.S.; resources, Z.-X.S., Q.-B.W. and G.-L.Z.; data curation, Z.-X.S.; writing—original draft preparation, Z.-X.S., Y.-Y.J., N.-W.Z., Q.-B.W. and G.-L.Z.; writing—review and editing, Z.-X.S., Q.-B.W. and G.-L.Z.; visualization, Z.-X.S., Q.-B.W. and G.-L.Z.; supervision, Z.-X.S., Q.-B.W. and G.-L.Z.; project administration, Z.-X.S. and Q.-B.W.; funding acquisition, Z.-X.S. and Q.-B.W. All authors have read and agreed to the published version of the manuscript.

**Funding:** This research was funded by the National Natural Science Foundation of China (No. 42277285), the Postdoctoral Research Foundation of China (No. 2018M640531), the National Natural Science Foundation of China (No. 41807002 and No. 41771245), the Special Foundation for National Science and Technology Basic Research Program of China (2021FY100405), the Scientific Research Fund of Liaoning Provincial Education Department (LSNQN202007) and the Department of Science and Technology of Liaoning Province (Liaoning Province Doctoral Startup Fund: No. 20170520407).

**Data Availability Statement:** All data are shown in the main manuscript.

**Acknowledgments:** The authors sincerely thank Phillip R. Owens, Zamir Libohova, and all the students who provided input to this study. Our acknowledgements also extend to the anonymous reviewers for their constructive reviews of the manuscript.

**Conflicts of Interest:** The authors declare no conflict of interest.

## References

1. Li, Y.; Shi, W.; Aydin, A.; Beroya-Eitner, M.A.; Gao, G. Loess genesis and worldwide distribution. *Earth-Sci. Rev.* **2020**, *201*, 102947. [[CrossRef](#)]
2. Liu, T.S. *Loess and the Environment*; China Ocean Press: Beijing, China, 1985; p. 251.
3. Gallet, S.; Jahn, B.-m.; Torii, M. Geochemical characterization of the Luochuan loess-paleosol sequence, China, and paleoclimatic implications. *Chem. Geol.* **1996**, *133*, 67–88. [[CrossRef](#)]
4. Smalley, I.J.; Marković, S.B.; Svirčev, Z. Loess is [almost totally formed by] the accumulation of dust. *Quat. Int.* **2011**, *240*, 4–11. [[CrossRef](#)]
5. Sprafke, T.; Obrecht, I. Loess: Rock, sediment or soil—What is missing for its definition? *Quat. Int.* **2016**, *399*, 198–207. [[CrossRef](#)]
6. Smalley, I.J.; Marković, S.B. Loessification and hydroconsolidation: There is a connection. *Catena* **2014**, *117*, 94–99. [[CrossRef](#)]
7. Ruhe, R.V. Relation of Fluctuations of Sea Level to Soil Genesis in the Quaternary. *Soil Sci.* **1965**, *99*, 23–29. [[CrossRef](#)]
8. Lehmkuhl, F.; Nett, J.J.; Pötter, S.; Schulte, P.; Sprafke, T.; Jary, Z.; Antoine, P.; Wacha, L.; Wolf, D.; Zerboni, A.; et al. Loess landscapes of Europe—Mapping, geomorphology, and zonal differentiation. *Earth-Sci. Rev.* **2021**, *215*, 103496. [[CrossRef](#)]

9. An, Z.S.; Kukla, G.J.; Porter, S.C.; Xiao, J.L. Magnetic susceptibility evidence of monsoon variation on the Loess Plateau of central China during the last 130,000 years. *Quat. Res.* **1991**, *36*, 29–36. [[CrossRef](#)]
10. Liu, T.S.; Guo, Z.T.; Liu, J.Q.; Han, J.M.; Ding, Z.L.; Gu, Z.Y.; Wu, N.Q. Variations of eastern Asian monsoon over the last 140,000 years. *Bull. Soc. Géol. Fr.* **1995**, *166*, 221–229.
11. Kukla, G.; An, Z.S. Loess stratigraphy in central China. *Palaeogeogr. Palaeoclimatol. Palaeoecol.* **1989**, *72*, 203–225. [[CrossRef](#)]
12. Ding, Z.; Yu, Z.; Rutter, N.; Liu, T. Towards an orbital time scale for Chinese loess deposits. *Quat. Sci. Rev.* **1994**, *13*, 39–70. [[CrossRef](#)]
13. An, Z.S. The history and variability of the East Asian paleomonsoon climate. *Quat. Sci. Rev.* **2000**, *19*, 171–187. [[CrossRef](#)]
14. Sun, Y.B.; Lu, H.Y.; An, Z.S. Grain size of loess, palaeosol and Red Clay deposits on the Chinese Loess Plateau: Significance for understanding pedogenic alteration and palaeomonsoon evolution. *Palaeogeogr. Palaeoclimatol. Palaeoecol.* **2006**, *241*, 129–138. [[CrossRef](#)]
15. Makeev, A.O. Pedogenic alteration of aeolian sediments in the upper loess mantles of the Russian Plain. *Quat. Int.* **2009**, *209*, 79–94. [[CrossRef](#)]
16. Zhou, L.P.; Oldfield, F.; Wintle, A.G.; Robinson, S.G.; Wang, J.T. Partly pedogenic origin of magnetic variations in Chinese loess. *Nature* **1990**, *346*, 737–739. [[CrossRef](#)]
17. Maher, B.A.; Thompson, R. Mineral magnetic record of the Chinese loess and paleosols. *Geology* **1991**, *19*, 3–6. [[CrossRef](#)]
18. Smalley, I.J. ‘In-situ’ theories of loess formation and the significance of the calcium-carbonate content of loess. *Earth-Sci. Rev.* **1971**, *7*, 67–85. [[CrossRef](#)]
19. Yang, S.L.; Ding, F.; Ding, Z.L. Pleistocene chemical weathering history of Asian arid and semi-arid regions recorded in loess deposits of China and Tajikistan. *Geochim. Cosmochim. Acta* **2006**, *70*, 1695–1709. [[CrossRef](#)]
20. Sun, Z.-X.; Owens, P.R.; Han, C.-L.; Chen, H.; Wang, X.-L.; Wang, Q.-B. A quantitative reconstruction of a loess–paleosol sequence focused on paleosol genesis: An example from a section at Chaoyang, China. *Geoderma* **2016**, *266*, 25–39. [[CrossRef](#)]
21. Guo, Z.T.; Fedoroff, N.; An, Z.S. Genetic types of the Holocene soil and the Pleistocene paleosols in the Xifeng loess section in central China. In *Loess, Environment and Global Change*; Science Press: Beijing, China, 1991; pp. 93–111.
22. Guo, Z.T.; Liu, T.S.; Fedoroff, N.; Wei, L.Y.; Ding, Z.L.; Wu, N.Q.; Lu, H.Y.; Jiang, W.Y.; An, Z.S. Climate extremes in loess of China coupled with the strength of deep-water formation in the North Atlantic. *Glob. Planet. Chang.* **1998**, *18*, 113–128. [[CrossRef](#)]
23. Guo, Z.T.; Biscaye, P.E.; Wei, L.Y.; Chen, X.H.; Peng, S.Z.; Liu, T.S. Summer monsoon variations over the last 1.2 Ma from the weathering of loess-soil sequences in China. *Geophys. Res. Lett.* **2000**, *27*, 1751–1754. [[CrossRef](#)]
24. Bronger, A.; Heinkele, T. Micromorphology and genesis of paleosols in the Luochuan loess section, China: Pedostratigraphic and environmental implications. *Geoderma* **1989**, *45*, 123–143. [[CrossRef](#)]
25. Smalley, I.J.; Obrecht, I. The formation of loess ground by the process of loessification: A history of the concept. *Geologists* **2018**, *24*, 163–170. [[CrossRef](#)]
26. Hydrogeology Brigade of Liaoning Geology Bureau. *The Quaternary of Liaoning Province*; Geology Press: Beijing, China, 1983.
27. Zeng, L.; Yi, S.; Zhang, W.; Feng, H.; Lv, A.; Zhao, W.; Luo, Y.; Wang, Q.; Lu, H. Provenance of loess deposits and stepwise expansion of the desert environment in NE China since ~1.2 Ma: Evidence from Nd-Sr isotopic composition and grain-size record. *Glob. Planet. Chang.* **2020**, *185*, 103087. [[CrossRef](#)]
28. Li, L.; Li, G.K.; Li, T.; Yi, S.; Lu, H.; Hedding, D.W.; Chen, J.; Li, G. Tracking the Provenance of Aeolian Loess in Northeastern China by Uranium Isotopes. *Geochem. Geophys. Geosyst.* **2023**, *24*, e2022GC010715. [[CrossRef](#)]
29. Soil Survey Staff. *Keys to Soil Taxonomy*, 12th ed.; USDA, NRCS. U.S. Gov. Print. Office: Washington, DC, USA, 2014.
30. Schoeneberger, P.J.; Wysocki, D.A.; Benham, E.C.; Soil-Survey-Staff. *Field Book for Describing and Sampling Soils*; Version 3.0; Natural Soil Survey Center: Lincoln, NE, USA, 2012.
31. Chen, H.; Wang, Q.B.; Han, C.L.; Wu, D.L. Grain-size distribution and material origin of a paleosol sequence at Fenghuang Mountain, Chaoyang, Liaoning Province. *Earth Environ.* **2009**, *37*, 243–248.
32. Lisiecki, L.E.; Raymo, M.E. Plio-Pleistocene climate evolution: Trends and transitions in glacial cycle dynamics. *Quat. Sci. Rev.* **2007**, *26*, 56–69. [[CrossRef](#)]
33. Cesaro, R. *X-ray Fluorescence Spectrometry*; Wiley Online Library: Hoboken, NJ, USA, 2010.
34. Murphy, C.P. *Thin Section Preparation of Soils and Sediments*; AB Academic: Berkhamsted, UK, 1986.
35. Bullock, P.; Fedoroff, N.; Jongerius, A.; Stoops, G.; Tursina, T. *Handbook for Soil Thin Section Description*; Waine Research: Wolverhampton, UK, 1985.
36. Brasher, B.R.; Franzmeier, D.P.; Valassis, V.; Davidson, S.E. Use of saran resin to coat natural soil clods for bulk density and water retention measurements. *Soil Sci.* **1966**, *101*, 108. [[CrossRef](#)]
37. Nelson, D.W.; Sommers, L.E. Total carbon, organic carbon, and organic matter. In *Methods of soil analysis. Part 2. Chemical and microbiological properties*; John Wiley & Sons, Ltd.: Hoboken, NJ, USA, 1982; pp. 539–579.
38. Lu, H.Y.; An, Z.S. An experimental study on the effect of pretreatment methods for the particle size determination of loess sediment. *Chin. Sci. Bull.* **1997**, *42*, 2535–2538.
39. Chen, H.; Wang, Q.B.; Han, C.L. Grain-size characteristics and climatic changes of a paleosol sequence at Fenghuang Mountain in Chaoyang, Liaoning Province. *Geol. J. China Univ.* **2009**, *15*, 563–568.
40. Kukla, G.; An, Z.S.; Melice, J.L.; Gavin, J.; Xiao, J.L. Magnetic susceptibility record of Chinese loess. *Trans. R. Soc. Edinb. Earth Sci.* **1990**, *81*, 263–288. [[CrossRef](#)]

41. Chen, H. Grain-Size Characteristics and Paleoclimatic Reconstruction during the Late Middle Pleistocene and the Last Interglacial Stage of a Paleosol Sequence at Fenghuang Mountain in Chaoyang, Liaoning Province. Ph.D. Thesis, College of Land and Environment, Shenyang Agricultural University, Shenyang, China, 2009. (In Chinese).
42. Sun, Z.X.; Wang, Q.B.; Han, C.L.; Zhang, Q.J.; Owens, P.R. Clay mineralogical characteristics and the paleoclimatic significance of a Holocene to Late Middle Pleistocene loess-paleosol sequence from Chaoyang, China. *Earth Environ. Sci. Trans. R. Soc. Edinb.* **2016**, *106*, 185–197.
43. Torrent, J.; Schwertmann, U.; Fechter, H.; Alferez, F. Quantitative relationships between soil color and hematite content. *Soil Sci.* **1983**, *136*, 354–358. [[CrossRef](#)]
44. Sun, Z.-X.; Jiang, Y.-Y.; Wang, Q.-B.; Owens, P.R. Geochemical characterization of the loess-paleosol sequence in northeast China. *Geoderma* **2018**, *321*, 127–140. [[CrossRef](#)]
45. Feng, J.-L.; Hu, H.-P.; Chen, F. An eolian deposit–buried soil sequence in an alpine soil on the northern Tibetan Plateau: Implications for climate change and carbon sequestration. *Geoderma* **2016**, *266*, 14–24. [[CrossRef](#)]
46. Rudnick, R.L.; Gao, R. Composition of the continental crust. *Crust* **2003**, *3*, 1–64.
47. Li, T.J.; Zhao, Y.; Zhang, K.L.; Zheng, Y.S.; Wang, Y. *Soil Geography*; Higher Education Press: Beijing, China, 2005.
48. Peng, B.Z.; Zhou, S.L. Several Questions in the Study of Paleosols. In *Soil Environmental Change*; Gong, Z.T., Ed.; China Science and Technology Press: Beijing, China, 1992; pp. 121–124.
49. Bronger, A.; Catt, J.A. Paleosols: Problems of definition, recognition and interpretation. *Catena Suppl.* **1989**, *16*, 1–7.
50. Duchaufour, P. *Pedology: Pedogenesis and Classification*; George Allen and Unwin: London, UK, 1982.
51. Xu, S.R. Understanding the relationship between environmental change and soil formation. In *Soil Environmental Change*; Gong, Z.T., Ed.; China Science and Technology Press: Beijing, China, 1992; pp. 118–120.
52. Lu, J.G.; He, L.M. The dimensional differentiation of paleogeneic red soil characters in eastern China. In *Soil Environmental Change*; Gong, Z.T., Ed.; China Science and Technology Press: Beijing, China, 1992; pp. 91–96.
53. Yaalon, D.H. The soils we classify essay review of recent publications on soil taxonomy. *Catena* **1995**, *24*, 233–241. [[CrossRef](#)]
54. Cremeens, D.L.; Brown, R.B.; Huddleston, J.H. *Whole Regolith Pedology*; Soil Science Society of America: Madison, WI, USA, 1994.
55. Nesbitt, H.; Young, G. Early Proterozoic climates and plate motions inferred from major element chemistry of lutites. *Nature* **1982**, *299*, 715–717. [[CrossRef](#)]
56. Li, X.; Han, Z.; Yang, S.; Chen, Y.; Wang, Y.; Yang, D. Chemical weathering intensity and element migration features of the Xiashu Loess profile in Zhenjiang. *Acta Geogr. Sin.* **2007**, *62*, 1174–1184. (In Chinese)
57. Kang, J.C.; Mu, D.F. Geochemical characteristics of beiyuan loess profile in Linxia city, Gansu, China. *J. Lan Zhou Univ.* **1998**, *34*, 119–125, (In Chinese with an English Abstract).
58. Ložek, V. Molluscan fauna from the loess series of Bohemia and Moravia. *Quat. Int.* **2001**, *76*, 141–156. [[CrossRef](#)]
59. Porter, S.C.; An, Z.S. Correlation between climate events in the North Atlantic and China during the last glaciation. *Nature* **1995**, *375*, 305–308. [[CrossRef](#)]
60. Yang, S.L.; Ding, Z.L. Comparison of particle size characteristics of the Tertiary ‘red clay’ and Pleistocene loess in the Chinese Loess Plateau: Implications for origin and sources of the ‘red clay’. *Sedimentology* **2004**, *51*, 77–93. [[CrossRef](#)]
61. Ding, Z.L.; Derbyshire, E.; Yang, S.L.; Yu, Z.W.; Xiong, S.F.; Liu, T.S. Stacked 2.6-Ma grain size record from the Chinese loess based on five sections and correlation with the deep-sea  $\delta^{18}\text{O}$  record. *Paleoceanography* **2002**, *17*, 5-1–5-21. [[CrossRef](#)]

**Disclaimer/Publisher’s Note:** The statements, opinions and data contained in all publications are solely those of the individual author(s) and contributor(s) and not of MDPI and/or the editor(s). MDPI and/or the editor(s) disclaim responsibility for any injury to people or property resulting from any ideas, methods, instructions or products referred to in the content.